2017 IEEE International Conference on Robotics and Automation (ICRA)
Singapore, May 29 - June 3, 2017

A Robotic Manipulator Design with Novel Soft Actuators

Xiaojiao Chen, *Student Member, IEEE*, Jing Peng, Jianshu Zhou, Yonghua Chen, Michael Yu Wang, *Fellow, IEEE*, and Zheng Wang*, *Senior Member, IEEE*

***Abstract*— Soft robots are inherently compliant and adaptive, therefore they are promising candidates for interacting with humans. However robotic manipulators utilizing soft actuators are often constrained by a series of actuator performance limitations. In this work we design a novel linear soft robotic actuator with significantly improved performances over the existing products, achieving 300% deformation ratio, quasi-constant output force over a wide motion range, while maintaining passive compliance and adaptability. Moreover, the novel actuator is less prone to friction, and could be fabricated using inject molding and 3D printing, hence having high repeatability at very low cost. An analytical model was developed to characterize the actuator behavior and provide a guideline for actuator design according to performance specifications. A 6 DOF soft manipulator was designed and fabricated utilizing the novel soft actuator. The manipulator arm had a serial kinematic structure with a biomimetic wrist and was driven by 12 soft actuators mounted onto the arm links. With 1.2m workspace radius and 1kg payload, the working air pressure could be as low as 1bar. Preliminary results have shown the validity of the novel soft actuator and manipulator designs, as well as the strong potential of soft robots in human-oriented applications.**

I. INTRODUCTION

The majority of robotic manipulators today are driven by electric motors, with gear-boxes to provide high torque output. However, gear reduction resulted in high mechanical impedance, therefore the manipulator rigidly follows the desired trajectory without adapting to environmental changes. Although special arrangements could be made, including interaction-monitoring sensors and advanced control algorithms, to achieve behavioral compliance, the complexity and cost of the system will be further increased [1-3].

Soft robotics [4-6] offers a different approach to electric-motor-based robotic manipulators by focusing more on human-centered metrics like safety, adaptability, compliance, and affordability. Pneumatic Artificial Muscles (PAM), also called McKibben muscles, are widely used [7-9] in antagonistic configurations to gain variable stiffness ability. The effectiveness of driving multi-DOF manipulators using PAMs were explored in many applications [10-11]. Comparing with existing rigid manipulators with safety functions, such as impedance controlled robots [12], or robots with direct-drive current-controlled joints [13], the soft manipulators achieved inherent and passive safety with simplified joint structure and little controller effort. However further development and improvement of soft robotic manipulators are limited by the performance constraints of PAMs, which had a theoretical maximum contraction ratio of approximate 30%, with a quickly decaying output force profile away from its natural resting length [14,15]. Therefore, the trade-off between the working range and the output force is always an issue for the design of this kind of robot arm [16].

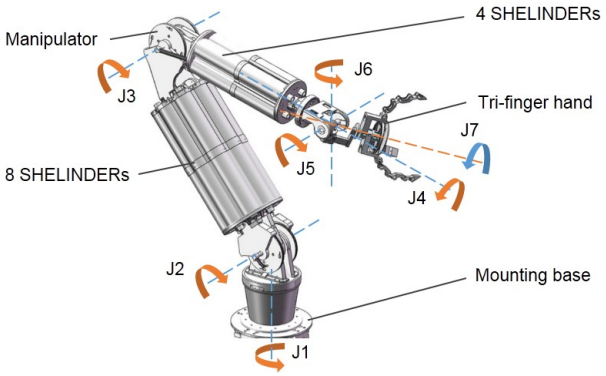

Fig. 1. The proposed robot manipulator consists of a 6 DOF arm and a tri-finger hand, driving by 12 novel pneumatic actuators,SHELINDER, through cable-sheath mechanism.

In this work, we first present a novel linear soft actuator design. The actuator design comprises of an external reinforcement shell enclosing an internal soft cylinder, hence given the acronym SHELINDER (SHEll + cyLINDER). The main design aims of SHELINDER are: 1) substantially increase the range of motion, 2) improve output force profile to be more linear over a wide motion range, 3) provide passive return force to the neutral position, 4) maintain inherent compliance and adaptability, 5) low actuation pressure requirement, 6) light weight and low fabrication cost. Utilizing the novel soft actuator, we designed a 6 DOF soft robotic manipulator arm, as shown in Fig.1. Each DOF was driven by two SHELINDERs in an antagonistic configuration, similar to existing bionic robot manipulator designs. The soft arm has the following design aims: 1) comparable or larger workspace than a human arm, 2) sufficient dexterity and payload for everyday tasks, 3) low working air pressure, 4) low mechanical impedance both at end-effector and on joints, 5) light weight and low cost.

In Section II the design of SHELINDER will be presented, together with the analytical model to describe its

X. Chen, J. Peng, J. Zhou, Y. Chen and Z. Wang are with the Department of Mechanical Engineering, the University of Hong Kong, Pokfulam, Hong Kong SAR, China

M. Wang is with the Department of Mechanical and Aerospace Engineering, the Hong Kong University of Science and Technology, Hong Kong SAR, China

Z. Wang is also with the University of Hong Kong Shenzhen Institute of Research and Innovation (HKU-SIRI), Shenzhen, China

*Corresponding author. Tel: +852-3917-7905, Fax: +852-2858-5415, zwangski@hku.hk

Chamber diameter (De)	62mm
Effective diameter (Di)	51mm
Maximum chamber length	400mm
Minimum chamber length	100mm
Number of segments (n)	45
Initial segment angle (α)	80°
Thickness of inner chamber (τ)	1mm
Outer shell length	450 mm
Maximum extention max (ϵ)	300%
Working pressure (P)	1bar
Maximum output force (F)	200N

TABLE I
SHELINDER DESIGN PARAMETERS

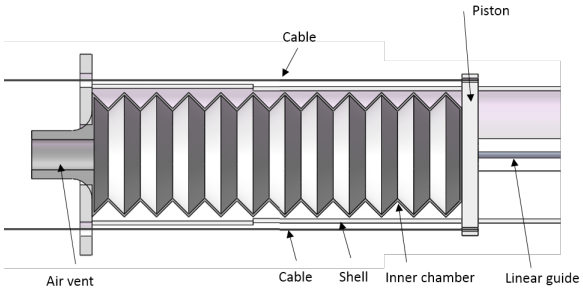

Fig. 2. SHELINDER uses inner chamber to hold air, and is restrained by the outer shell. The pushing force is conveyed by driving piston upward who is also constrained by linear guideway.

performances. The design of the 6 DOF soft arm will be presented in Section III, together with the design of an extremely low weight robotic hand to be integrated with the arm. Experiments and preliminary test results on the fabricated SHELINDER will be given in Section IV, followed by conclusions and future work in Section V.

II. SOFT ACTUATOR DESIGN AND MODELING

A. Design of soft actuator SHELINDER

Pneumatic driven soft robotic actuators have a similar fundamental mechanism for motion creation, where an expandable internal chamber is inflated by the supplied pressurized air, while external constraining mechanisms, such as features on the chamber wall, inextensible fibers, sheets, and flexible beams, selectively constrain the chamber expansion into the desirable manner, hence generate the actuator motion. The McKibben muscle generates linear contractile motion from the inner chamber expansion with an external constraining layer of meshed fiber, which redirects radial expansion to axial contraction. As a result, both the contractile motion and the axial output force are affected by the pitch of the fiber mesh, such that the maximum theoretical contraction ratio is around 30%, and even less in practice, while the maximum output force only occurs at the original length (0% contraction), and drops quickly to below 1/2 of the maximum value at only 10% contraction. Friction loss is also significant, as the chamber is always pressing against the fiber mesh during actuation, producing a high normal force and in turn significant friction forces both inter-fiber and between fiber and the air chamber [17].

In this work we took a different approach in soft actuator design: the actuator comprises of a cylindrical air chamber and encircling constraining components; 1) the inner chamber is self-constrained radially and deformable between a minimum and a maximum length axially; 2) the external components use flexible cables to redirect the axial extension into axial contraction. The actuator design is illustrated in Fig. 2. For the inner chamber, a classical bellow structure is used, with the distal end closed and the proximal end open to an air vent, as shown in Fig.2. The chamber is fabricated from flexible but inextensible thin film material. The circumferential ring-shaped edge on each folding segment S serves as a constraint to radial expansion. Along the axial direction, however, the bellow structure will exhibit two distinctive behaviors: 1) if expanded axially from its original length, the concave portions of the bellow wall will be stretched, hence the axial elongation will be minimal and subject to the extensibility of the material used to fabricate the chamber; 2) if compressed axially from its original length, the concave portions will easily buckle due to material flexibility, and the bellow structure will collapse and contract axially with a minor resistance force, which will increase as the contraction continues, until eventually the adjacent chamber walls are in contact and the actuator reaches the minimum length.

The cylindrical outer shell has the proximal end closed to mount the proximal end of the inner chamber, with three holes: two for passing cables and one for passing the tubing connecting to the air vent of the inner chamber. The distal end of the shell is open with a piston freely sliding axially along a linear guide. The piston is fixed to the distal end of the air chamber. Two flexible but inextensible cables are fixed to opposing edges of the piston, and pass through the two holes on the proximal end of the outer shell and connect to the external payload. The outer shell has a slightly larger inner diameter than the outer diameter of the inner chamber, such that no contact is expected during the actuation. The intended operating setup for SHELINDER is to use two SHELINDERs to drive one joint forming an antagonistic configuration. The output force from the actuator is transmitted to drive the pulley in the robotic joint using flexible cable-sheath transmission [18]. The sheath connecting the SHELINDERs proximal end and the joint is flexible but incompressible, therefore transmitting the compression forces while maintaining flexibility on the transmission path. Initially, both SHELINDERs are at a neutral position (typically 50% of the usable deformation range), and the joint is also at its neutral angle, as shown in Fig.3 (a). When one SHELINDER is pressurized, it will extend axially and pull the cables from the sheath, turn the joint, and hence the cables connecting to the antagonistic SHELINDER will compress the opposing actuator passively, as shown in Fig.3 (b) and Fig.3 (c).

B. Comparison to existing technologies

In the intended antagonistic application, the proposed SHELINDER has substantial advantages over existing soft

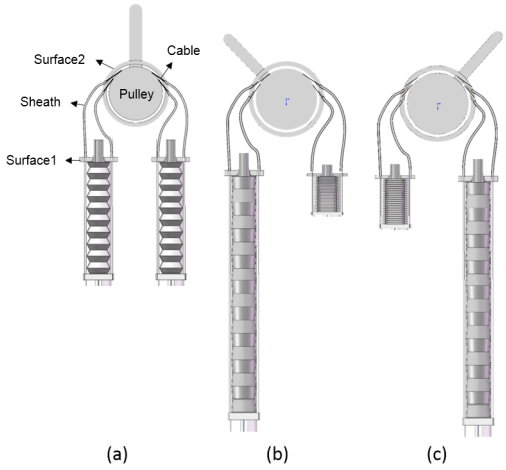

Fig. 3. Different working configurations of antagonistic SHELINDERS: (a) Balance state when two SHELINDERs are both in their middle position; (b) Agonistic SHELINDER is inflated and antagonistic SHELINDER is delfated, the pulley will be drived counterclockwise; (c) Antagonistic SHELINDER is inflated and agonistic SHELINDER is delfated, the pulley will be drived clockwise.

actuators. 1) revolutionary increase in motion range, with the bellow structure, SHELINDER could achieve over 300% deformation in comparison with 30% for the McKibben muscle, as can be seen in Fig.4; 2) output force in theory will be constant throughout the entire motion range, with minimal attenuation due to the passive return force from the bellow structure, this is a huge improvement over the quick force drop with contraction for McKibben muscles; 3) friction can be minimized by applying sufficient lubrication; 4) passive compliance and adaptability can be achieved by SHELINDERs similar to McKibben muscles; 5) with the wide motion range and constant force output, the mechanical impedance of the antagonistic joint can be controlled by regulating the co-contracting level of the two SHELINDER actuators similar to McKibben muscles. The SHELINDERs extending motion is to some extent similar to the classic pneumatic cylinders. However, there are substantial differences: 1) the air cylinder requires a rigid shell to withstand internal pressure, while the SHELINDER has a flexible chamber to withstand pressure and not in contact with the outer shell; 2) the air cylinders piston is a crucial part in preventing air leakage, while the SHELINDER is inherently air-tight thanks to the unified and closed air chamber, the piston is simply offering cable connection; 3) the air cylinder has a rigid shaft that slides inside the cylinder, hence the maximum theoretical extension ratio is 100%, while the SHELINDER, with its flexible transmission mechanisms, could easily achieve 300% extension in practice; 4) the force output for the air cylinder and the SHELINDER with the same dimensions should be similar.

C. Modeling of SHELINDER

In order to quantify and analyze the behaviors of the proposed SHELINDER actuator, an analytical model is developed in this section, based on its design and physical dimensions. The model provides relationships between the actuator extension, input pressure, and output force. It provides an analytical tool to investigate the quasi-static behavior of SHELINDER actuators.

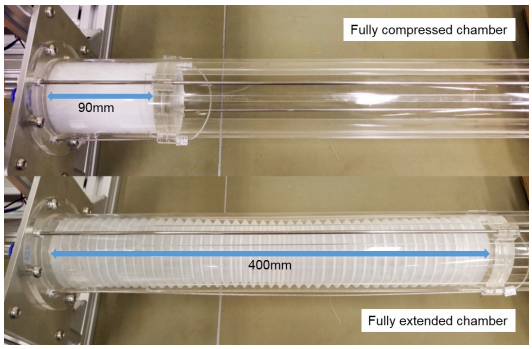

Fig. 4. SHELINDER has an impressive compression ability.

$$l = 2nB\sin(\frac{\theta_0}{2}) \tag{1}$$

$$\frac{D_e - D_i}{2} = B\cos(\frac{\theta_0}{2}) \tag{2}$$

$$l_{min} = 2n\tau \tag{3}$$

l is the actual length of SHELINDER. n is the number of segments. B is the width of the fold. $\theta_0$is the angle between two sequencing folds. τ is the thickness of the inner chamber. D_e and D_i are the outer diameter and active diameter separately. According to equation (1) and equation (3), we can get the elongation ratio of SHELINDER as

$$\epsilon = \frac{l - l_{min}}{l_{min}} = \frac{B}{\tau}\sin(\frac{\theta_0}{2}) - 1 \tag{4}$$

In fact, the force SHELINDER generates is related to the deformation ratio ϵ nonlinearly due to the energy storage and dissipation. When no pressure is applied, the force will increase along with the deformation. This phenomenon could be regarded as the self-damping-spring feature of SHELINDER. Experiments were conducted to measure this deformation generated force.

$$F = P\frac{\pi {D_i}^2}{4} + f(l) \tag{5}$$

The analytical models will be validated by comparing with experimental measurements in Section IV after the following further design description about the manipulator.

III. SOFT MANIPULATOR DESIGN

A. Kinematic structure

In order to achieve dexterity in a large workspace volume with a fixed mounting base, a serial kinematic structure is selected for this soft manipulator. In particular, the preliminary arm design in this work has 6 DOF to achieve arbitrary location and orientation placement within the reachable area without considering redundancy. On the other hand, due

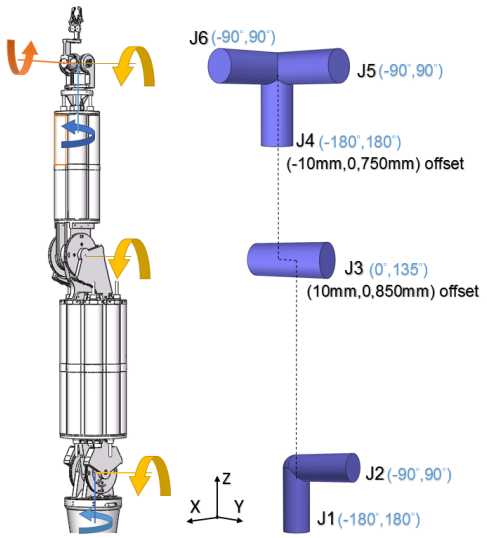

Fig. 5. Kinematic structure of the soft manipulator: a Z-Y-Y-Z-Y-X configuration.

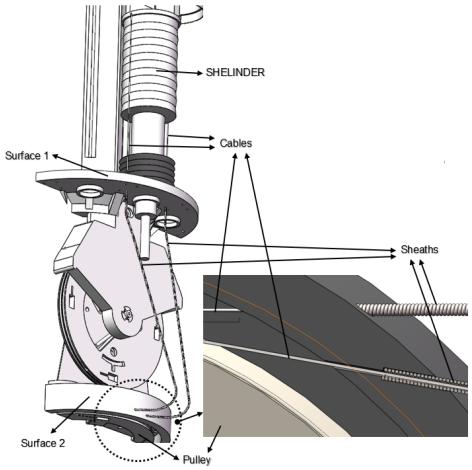

Fig. 6. The first joint J1 is along Z axis driven by two SHELINDERs. One SHELINDER is responsible for the rotation in one direction by two cables. The other SHELINDER is in the same configuration, in opposite direction.

to the flexible cable transmission used in the antagonistic actuation setup, it is possible to integrate multiple DOFs within a tight space and use cables to drive them individually without sacrificing performance significantly. Therefore, we proposed the kinematic structure for soft manipulator as shown in Fig.5. Three different types of joints are used in the arm: 1 dual-DOF rotational joint, 1 single-DOF rotational joint, and 1 triple-DOF wrist joint. The overall kinematics is in a Z-Y-Y-Z-Y-X configuration, with the first two joints intersecting and the last three joints intersecting. The joint type and axis parameters like rotation range and offset with respect to its previous joint are listed in Fig.5.

To reduce the gravity arm, the actuators are designed to be located near the base joint. With 6 DOF joints, a total of 12 SHELINDER actuators are required, out of which 8 are mounted on the first arm link driving the first four joints J1-J4, while 4 actuators are mounted on the forearm link to control the last two joints J5, J6. By using cable-sheath mechanism, the driving force could be easily transmitted from the actuators to their corresponding pulleys without introducing extra intermediate pulleys.

B. Design of soft manipulator

Each individual DOF of the soft manipulator is driven by two SHELINDERs antagonistically, an illustration of which is shown in Fig.3. As one SHELINDER gives out two cables, both of which goes through two separate holes on surface1 and surface2, between which a sheath is used to guide and support the cables. The cables are then attached to the pulley clockwise. The antagonistic SHELINDER is in the same configuration, except that the cable is attached to the pulley counter clockwise. The sheath made of helical steel is bendable but incompressible, enabling flexible transmission path without affecting cable position. Therefore, the cable-sheath can reach anywhere in the space without the need of complimentary pulleys to guide the direction, which gives more flexibility and reduces the structural complexity of the system.

The first joint J1 connects the first link to the mounting base in a rotational joint along Z axis. It has one pulley on which 4 cables are attached, while the other 5 joints are all equipped with two pulleys for more balanced pulling forces. From Fig.6, we can see that one particular SHELINDER gives out two cables, who goes through sheaths and reaches the pulley who is fixed to the base. The length of the cable could be regarded as four parts, with part 1 from SHELINDER piston to surface1, part 2 from surface1 to surface2, part 3 from surface2 to pulley, and part 4 attached on the pulley. When this SHELINDER is inflated, it will drive the piston up, resulting the length of part 1 to increase. Since the sheath is incompressible, and surface2 has a constant distance to the pulley, cable length in part 2 and part 3 is unchanged. Therefore it could only be part 4, cable attached on to the pulley, that is shortened, which means a relative rotation between the pulley and the surface2, who is part of the following link. Thus, this SHELINDER generates rotation in one direction between base and link1. On the opposite side, the other SHELINDER generates the counter directional rotation.

The second joint J2 is a rotational joint along Y axis. It intersects with the first joint. Unlike the first joint, it has two pulleys fixed to both ends of a common shaft to mount the 4 cables. Two cables from actuators are separately attached onto the two pulley both clockwise, while the counterparts from the other actuator counterclockwise. Since this joint has to burden the gravity of the manipulator, two torsion springs are used to compensate for the gravity.

The elbow joint J3 is also a rotational joint along Y axis. In order to increase the working range of the manipulator, J3 has an off-set to the line which goes through the intersecting point of the first two joints and the intersecting point of the last three joints. This offset enables the forearm link to have a 135 degree maximum rotary range relative to the previous

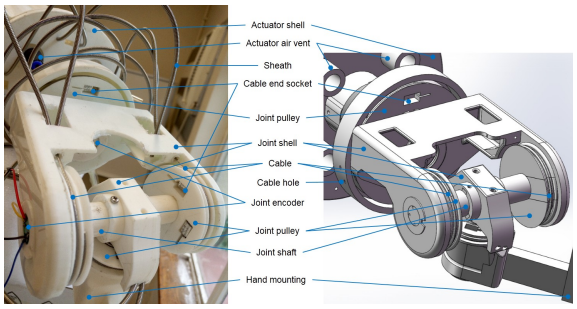

Fig. 7. Structure of the last three intersecting joints.

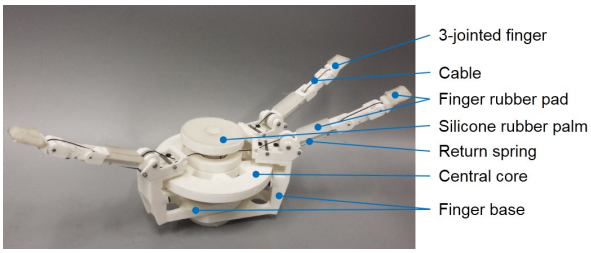

Fig. 8. The tri-fingered hand provides an additional degree of freedom of wrist rotation by turning three fingers synchronously.

arm link without collision.

The last 3 joints intersect at one common point, forming an omnidirectional wrist mimicking the human biological wrist. This feature enables the manipulators reachable space to be the same as the dexterous space [19]. The design of the 3 intersecting joints driven by cable-sheath mechanism is illustrated in Fig.7.

Eight SHELINDERs are mounted onto the link between J2 and J3 to drive the first 4 joints. They are arranged in a circular mode around a central carbon fiber tube providing structural support. The remaining four SHELINDERs are mounted onto the link between J3 and J4 to actuate the last 2 joints J5-J6. They are also arranged in a circular mode around a central supporting tube. Given the sheer size of the forearm, there are marginal space for mounting further actuators and other mechanisms.

To measure joint angles, all six joints are equipped with absolute encoders. Off-the-shelf encoders (Mini4096J) are used on J1-J3, while permanent magnets are embedded on the shafts of J4-J6 because of the tight space, and 3 pieces of AMS5048A ICs are used to detect the absolute angle.

C. Design of a rotational tri-finger robotic hand

In the final phase of manipulator design, we propose a novel design of a robotic end-effector with three robotic digits mounted on a rotational frame, to achieve an additional DOF at the end of the manipulator, while providing advanced tri-finger grasping functionalities. The concept includes: 1) a fixed core mounting the hand to the robotic arm as structural support; 2) three finger bases attaching to the core, each being able to rotate around the central axis of the core independently; 3) each finger base could mount a robotic finger, which can bend and perform grasping functions; 4) actuators driving the finger base rotation and finger bending could be mounted either on the hand, or on the forearm into the manipulator to reduce end-effector weight and improve grasping performance.

A conceptual design of the tri-fingered robotic hand is shown in Fig.8. The three fingers each have three rotational joints driven by one cable for bending, and equipped with back-mounting springs for passive return. The three fingers are mounted to the core and could rotate independently around it. As a result, rotating the three fingers simultaneously at the same speed would be equivalent to having an additional rotational DOF along the Z axis at the tip of the manipulator. Integrating the soft arm with the tri-fingered hand, the overall manipulator will have 7 DOFs and hence achieve redundancy and also a larger dexterous space.

The overall manipulator has a weight of approximate 5kg which is lighter than the 7 DOF robot arm designed by Tondu et al. The 1bar working pressure is also lower than 6bar which is common in most situations. The cable-sheath mechanism is quite different from commonly used belt or chain transmission, avoiding usage of additional intermediate pulleys or complex structures.

IV. EXPERIMENTAL VALIDATION

This section presents fabrication and validation results on the proposed SHELINDER actuator and the soft manipulator. 200 inner chambers were fabricated by inject molding using flexible polyvinyl chloride. Push-in tubing connectors were fitted to each chamber as air vent. The inject-molding process ensured excellent sample repeatability and stability of the chambers, while also achieved a fabrication cost of as low as US $0.2 per piece. The complete soft manipulator, including the arm and the tri-fingered hand, were fabricated, mostly us-

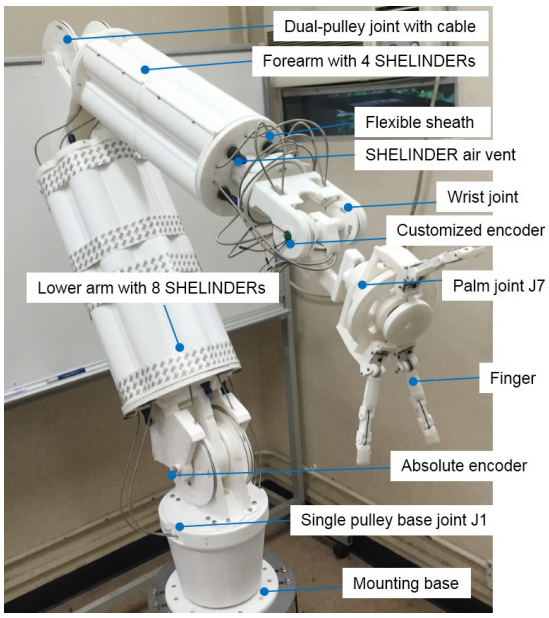

Fig. 9. The whole manipulator is all 3d printed except for necessary ball bearing and fastens.

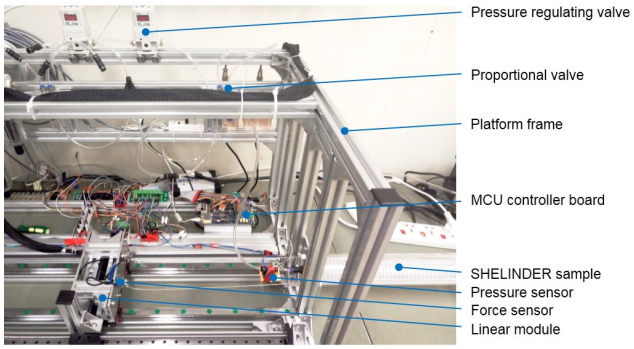

Fig. 10. Dedicated platform for testing SHELINDER.

ing 3D-printing of polylactide, reinforced by carbon fiber and metallic auxiliary components. Air tubing, angular encoders, driving cables and transmission sheathes were all fitted as previously presented.

A dedicated experimental platform was built to test the characteristics of SHELINDER as shown in Fig.10. In the platform, a pressure valve (SMC ITV2030) is used to regulate the supplied air pressure to the system. A proportional directional valve (Festo MPYE-5-1/8-HF-010-B) is used to control the flow rate and direction of the air into the SHELINDER. Pressure sensors (Honeywell HSCDANN060PGSA3) were mounted as close as possible to the inlet of the SHELINDER to monitor the pressure within the actuator with a resolution of 0.2kPa. Two force sensors (Forsentek FL25) were used to see the individual forces on the cables of one SHELINDER with a resolution of 1N. A linear module driven by step motor was used for motion generation, where a magnetic incremental linear sensor (RLS LM10) was used to provide reliable position control with an accuracy up to 1 um. The platform was controlled by STM32F429IGT, a 32-bit MCU based on ARM Cortex-M4 with a clock frequency up to 180MHz.

In the first experiment, a SHELINDER was mounted horizontally on the experimental platform, with the two cables connecting to the force sensor. Under the ambient pressure,

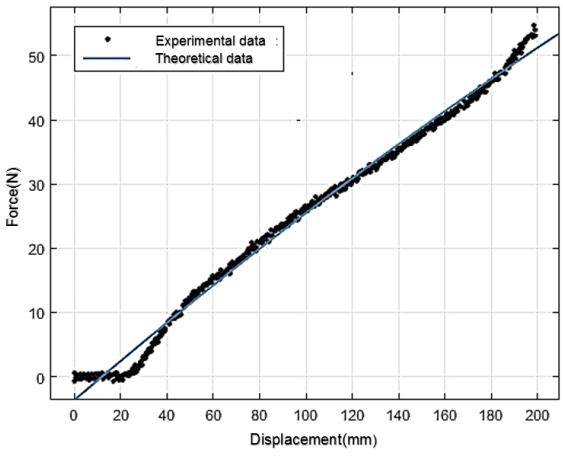

Fig. 11. Force-displacement relationship without pressurised air

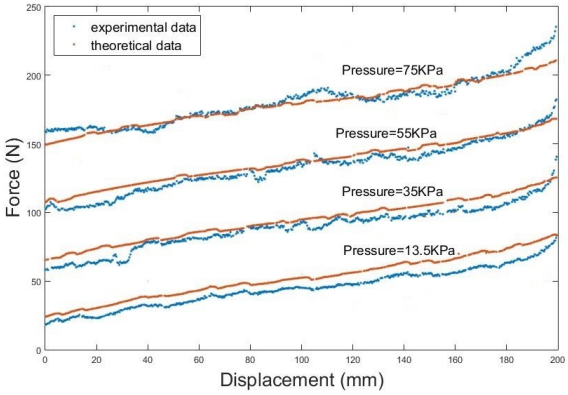

Fig. 12. Force-displacement relationship under different pressure.

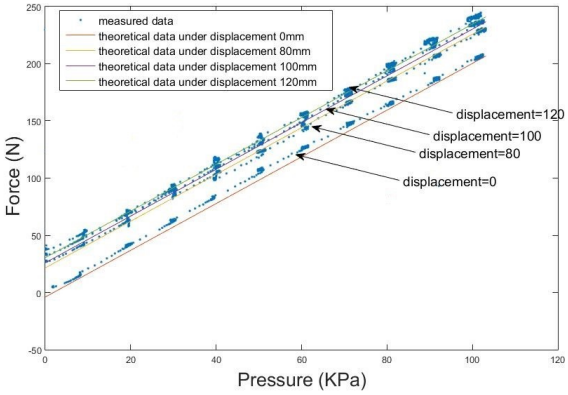

Fig. 13. Force-pressure relationship under different position.

the step motor drive SHELINDERs cables in a linear speed very slowly. The corresponding force were measured and could be fitted by a linear line in the large range, as shown in Fig.11. The fitted equation is:

$$f(x) = 0.274x - 3.3 \tag{6}$$

Where x represents the displacement towards the contraction direction, origin defined at the maximum rest length. The y-intercept is not identical to zero here because of the tested SHELINDER has shifted its rest length a little due to material memory characteristic. Thus the SHELINDER possesses a constant intrinsic stiffness within a certain range, and the overall analytical model could be written as

$$F = P\frac{\pi {D_e}^2}{4} + 0.274x - 3.3 \tag{7}$$

The analytical model was used to calculate the force using the measured pressure from the experiment. Comparisons of the analytical modeling results and the experimental measurements are presented in Fig.12. The analytical model was successful in predicting the behavior of the actuator by producing results showing very good agreement with experimental measurements in all pressure conditions. The y-intercept represents the force generated by pressure purely,

since at this moment the SHELINDER is not compressed, generating zero intrinsic spring force. At almost maximum displacement, the spring effect would increase significantly due to material incompressible characteristics.

The second experiment was focused on force behavior with pressure under different position. Results are shown in Fig.13. It reveals that a linear relationship exists between pressure and force under certain displacement. And the slope represents the effective area. The y-intercept corresponds well to the zero-pressure force-displacement data. These curves illustrate the passive and potential active compliance ability of SHELINDER. When pressure is zero, meaning in ambient pressure, certain displacement would result in a return force. This represents the minimum stiffness that the SHELINDER exhibits. By adjusting pressure, larger return force could be gained at the same displacement, meaning a controllable stiffness could be achieved.

V. CONCLUSION AND FUTURE WORK

In this paper, we presented a novel soft robotic actuator SHELINDER, aiming at driving robotic joints in antagonistic configurations. By introducing inherent motion constraints and innovations in outer mechanism design, we could achieve over 10 times improvement over the classic McKibben actuator, as well as a quasi-constant output force profile over a wide range of extension motion, while maintaining passive compliance and adaptability. Moreover, the SHELINDER actuator could be fabricated using inject molding and 3D printing techniques, with a customizable design air chamber fabrication cost of as low as US$0.2 per piece with very high repeatability. We have also developed an analytical model for the SHELINDER actuator to characterize its quasi-static behavior, which was validated in the experiments using fabricated actuators. The proposed model was proven to provide very accurate results in comparison with the true actuator, it provides us with a simple and intuitive tool to analyze SHELINDER behavior as well as a guideline to actuator design according to the desired performances. Utilizing the significant performance improvements, we designed a complete soft robot manipulator with arm and hand driven by SHELINDER actuators. The manipulator had up to 7 DOFs with a biomimetic kinematic structure. The manipulator was fabricated using 3D-printed components with reinforcements and driven by SHELINDER actuators. With a 1.2m workspace and 1kg payload, the working air pressure is as low as 1bar.

In the next stage, dynamic performance of the SHELINDER actuator will be investigated, as well as engineering factors such as the fatigue and failure mode. Advanced control of the antagonistic joint will be implemented to achieve impedance regulation using two SHELINDERs. The preliminary soft manipulator prototype will be developed further, with control algorithms implemented towards richer functionalities both for the arm and the hand, in performing manipulation and interaction tasks. With the performance improvements of SHELINDER actuators, the soft manipulator has strong potential in offering an alternative approach to robotic manipulators for service robots and other human-centered applications.

REFERENCES

[1] Wang, Z., Peer, A. and Buss, M., 2009, March. An HMM approach to realistic haptic human-robot interaction. In EuroHaptics conference, 2009 and Symposium on Haptic Interfaces for Virtual Environment and Teleoperator Systems. World Haptics 2009. Third Joint (pp. 374-379). IEEE.

[2] Wang, Z., Peer, A. and Buss, M., 2009, April. Fast online impedance estimation for robot control. In Mechatronics, 2009. ICM 2009. IEEE International Conference on (pp. 1-6). IEEE.

[3] Kwon, D.S., Woo, K.Y. and Cho, H.S., 1999. Haptic control of the master hand controller for a microsurgical telerobot system. In Robotics and Automation, 1999. Proceedings. 1999 IEEE International Conference on (Vol. 3, pp. 1722-1727). IEEE.

[4] Majidi, C., 2014. Soft robotics: a perspectivecurrent trends and prospects for the future. Soft Robotics, 1(1), pp.5-11.

[5] Trivedi, D., Rahn, C.D., Kier, W.M. and Walker, I.D., 2008. Soft robotics: Biological inspiration, state of the art, and future research. Applied Bionics and Biomechanics, 5(3), pp.99-117.

[6] Wang, Z., Chen, M.Z. and Yi, J., 2015. Soft robotics for engineers. HKIE Transactions, 22(2), pp.88-97.

[7] Choi, T.Y., Choi, B.S. and Seo, K.H., 2011. Position and compliance control of a pneumatic muscle actuated manipulator for enhanced safety. IEEE Transactions on Control Systems Technology, 19(4), pp.832-842.

[8] Ugurlu, B., Forni, P., Doppmann, C. and Morimoto, J., 2015, September. Torque and variable stiffness control for antagonistically driven pneumatic muscle actuators via a stable force feedback controller. In Intelligent Robots and Systems (IROS), 2015 IEEE/RSJ International Conference on (pp. 1633-1639). IEEE.

[9] Andrikopoulos, G., Nikolakopoulos, G. and Manesis, S., 2011, June. A survey on applications of pneumatic artificial muscles. In Control & Automation (MED), 2011 19th Mediterranean Conference on (pp. 1439-1446). IEEE.

[10] Woods, B.K., Kothera, C.S., Wang, G. and Wereley, N.M., 2014. Dynamics of a pneumatic artificial muscle actuation system driving a trailing edge flap. Smart Materials and Structures, 23(9), p.095014.

[11] Tondu, B., Ippolito, S., Guiochet, J. and Daidie, A., 2005. A seven-degrees-of-freedom robot-arm driven by pneumatic artificial muscles for humanoid robots. The International Journal of Robotics Research, 24(4), pp.257-274.

[12] Caccavale, F., Chiacchio, P., Marino, A. and Villani, L., 2008. Six-dof impedance control of dual-arm cooperative manipulators. IEEE/ASME Transactions On Mechatronics, 13(5), pp.576-586.

[13] Mitsantisuk, C., Katsura, S. and Ohishi, K., 2010. Force control of humanrobot interaction using twin direct-drive motor system based on modal space design. IEEE Transactions on Industrial Electronics, 57(4), pp.1383-1392.

[14] Tondu, B., 2012. Modelling of the McKibben artificial muscle: A review. Journal of Intelligent Material Systems and Structures, 23(3), pp.225-253.

[15] Daerden, F. and Lefeber, D., 2002. Pneumatic artificial muscles: actuators for robotics and automation. European journal of mechanical and environmental engineering, 47(1), pp.11-21.

[16] Shin, D., Yeh, X. and Khatib, O., 2013. Circular pulley versus variable radius pulley: Optimal design methodologies and dynamic characteristics analysis. IEEE Transactions on Robotics, 29(3), pp.766-774.

[17] Davis, S. and Caldwell, D.G., 2006. Braid effects on contractile range and friction modeling in pneumatic muscle actuators. The International Journal of Robotics Research, 25(4), pp.359-369.

[18] Wang, Z., Sun, Z. and Phee, S.J., 2013. Modeling tendon-sheath mechanism with flexible configurations for robot control. Robotica, 31(07), pp.1131-1142.

[19] Davidson, J.K. and Hunt, K.H., 2004. Robots and screw theory: applications of kinematics and statics to robotics. Oxford University Press on Demand.